Effect of nanocomposite structure on the thermoelectric properties of 0.7-at% Bi-doped Mg_2Si nanocomposite*

Yang Mei-Jun(杨梅君)[a)b)†], Shen Qiang(沈 强)[b)], and Zhang Lian-Meng(张联盟)[b)]

[a)] *Centre for Materials Research and Analysis, Wuhan University of Technology, Wuhan* 430070, *China*

[b)] *State Key Laboratory of Advanced Technology for Materials Synthesis and Processing, Wuhan University of Technology, Wuhan* 430070, *China*

(Received 6 December 2010; revised manuscript received 10 June 2011)

Nanocomposites offer a promising approach to the incorporation of nanostructured constituents into bulk thermoelectric materials. The 0.7-at% Bi-doped Mg_2Si nanocomposites are prepared by spark plasma sintering of the mixture of nanoscale and microsized 0.7-at% Bi-doped Mg_2Si powders. Microstructure analysis shows that the bulk material is composed of nano- and micrograins. Although the nanograin hinders electrical conduction, the nanocomposite structure is more helpful to reduce thermal conductivity and increase the Seebeck coefficient, hence improving thermoelectric performance. A dimensionless figure of merit of 0.8 is obtained for the 0.7-at% Bi-doped Mg_2Si nanocomposite with 50-wt % nanopowder, which is about twice larger than that of the sample without nanopowder.

Keywords: intermetallic compounds, nanostructures, semiconductors, thermoelectric effects

PACS: 62.23.Pq **DOI:** 10.1088/1674-1056/20/10/106202

1. Introduction

Mg_2X (X=Si, Ge, Sn) compounds have attracted much attention as one of the most promising thermoelectric materials due to their low cost and nontoxicity.[1−3] The performance of thermoelectric materials can be characterized by the dimensionless figure of merit ZT and $ZT = (\alpha^2\sigma/\kappa)T$, where α is the Seebeck coefficient, σ and κ are the electrical conductivity and thermal conductivity, respectively, and T is the absolute temperature. Conventionally, heavy doping and solid solutions are regarded as common methods to improve thermoelectric properties of Mg_2Si, such as the doping of Sb, Te, Bi in Mg_2Si, Mg–Si–Sn, and Mg–Si–Ge systems, and so on.[4−7] The results of recent studies show that the thermoelectric performance of Mg_2Si material can be improved by inducing nanostructures due to the reduction of the thermal conductivity and the enhancement of the Seebeck coefficient.[8,9] The incorporation of nanoscale constituents into bulk material to form nanocomposites has also been proven to be an effective method to improve thermoelectric prosperities in some thermoelectric systems.[10−14] So far, there have been some reports on fabrication procedure, thermal stability, growth behaviour and mechanical properties of nanocrystalline Mg_2Si prepared by the mechanical alloying method,[15−18] but the effect of the nanostructure on the thermoelectric properties of Mg_2Si has drawn little attention.[19,20] In the present paper, the preparation and the thermoelectric properties of Mg_2Si nanocomposite fabricated by spark plasma sintering (SPS) of the mixture of nanoscale and microsized Mg_2Si powders are reported and the effect of the nanostructure on thermoelectric properties is intensively investigated.

2. Experiment

The initial microsized 0.7-at% Bi-doped Mg_2Si powder was synthesized by a spark plasma sintering system (SPS-1050) from Mg (325 mesh, 99.96%) and Si (300 mesh, 99.999%), and Bi (300 mesh, 99.999%) powders at 823 K–0 MPa for 10 min. A planetary ball milling machine was used with a vial rotation speed of 370 rpm to form nanosized Mg_2Si powder. The vial and balls were made of tungsten carbide (WC). The ball-to-powder ratio was 20:1. Consolidation of the mixture of microsized and nanoscale Mg_2Si pow-

*Project supported by the National Basic Research Program of China (Grant No. 2007CB607501) and the Fundamental Research Funds for the Central Universities.

†Corresponding author. E-mail: liyangmeijun@163.com

© 2011 Chinese Physical Society and IOP Publishing Ltd

ders was carried out in spark plasma sintering machine (SPS-1050) using graphite dies at a temperature up to 800 °C for 5 min under 50 MPa with a heating-rate of 100 °C/min. In the present study, the bulk nanocomposite samples by spark plasma sintering are denoted as "NX", where "X" is a number denoting the weight percentage of nanopowder in the sample.

Morphologies of microsized and nanoscale powders and the structure change of nanocomposite sample were characterized by transmission electron microscopy (TEM, JEM-2010, Japan) and field emission scanning electron microscopy (FESEM, S-4800). Phases of the powder were detected by X-ray diffraction (D/Max-RB, Japan). The average grain size of nanoscale Mg_2Si powder was evaluated by MDI Jade computer software based on the Scherrer formula.[22] The density of the sintered samples was measured by the Archimedes method. The Seebeck coefficient α and the electrical conductivity σ were measured simultaneously using ZEM-1 (Japan) apparatus in a temperature range from 300 K to 823 K. The Hall measurement of our nanocomposite at room temperature was carried out by an Accent HL5500PC system using the van der Pauw method. The thermal conductivity κ in a temperature range from 300 K to 823 K was calculated from the equation of $\kappa = D \times C_p \times d$, where d is the density of the specimen, the thermal diffusivity D and specific heat C_p were measured by a laser flash method (Shinkuriko: TC-7000, Japan).

3. Results and discussion

3.1. Phases and microstructure characterization

Figure 1 shows the typical XRD patterns of microsized and nanoscale Mg_2Si raw powders. The peaks are broader for the nanoscale Mg_2Si powder, which confirms the reduction of grain size, and the average grain size of the nanoscale powder is determined (by XRD) to be 25 nm. Figure 2 shows the FESEM and TEM images of the microsized and nanoscale Mg_2Si powders. The particle size of the microsized powder is about 3 μm (Fig. 2(a)), but for nanopowder (Fig. 2(b)) the particle size decreases dramatically, which accords with the result of XRD.

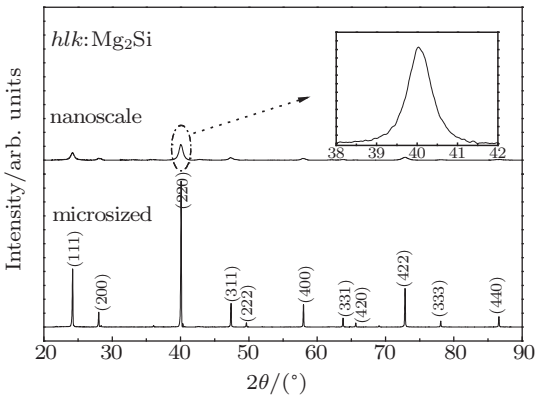


Fig. 1. XRD patterns of microsized and nanoscale Mg_2Si powders.

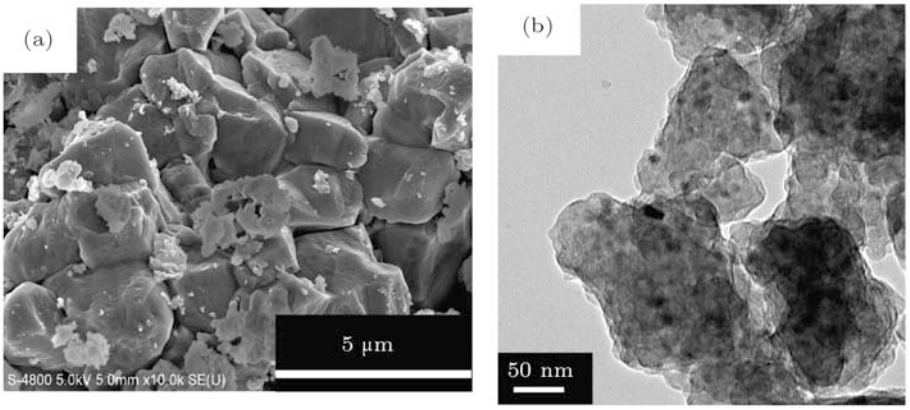


Fig. 2. FESEM and TEM of microsized and nanoscale Mg_2Si powders.

The FESEM and the TEM images of the fractured surface of the bulk samples of N0, N50 and N100 are shown in Fig. 3. It is clearly observed that the grains of the N0 and N100 samples each have a homogeneous distribution. No pores can be seen from the fractured images and the relative densities of the three samples are all nearly 100%. The N50 bulk material (Fig. 3(b)) is composed of nanocrystals with an average grain size of 100 nm and large microsized crystals. The results show that the obtained samples have nanocomposite structures. Other nanopowder-containing samples demonstrate similar nanocomposite structures with different ratios between the nanocrystal and microcrystal.

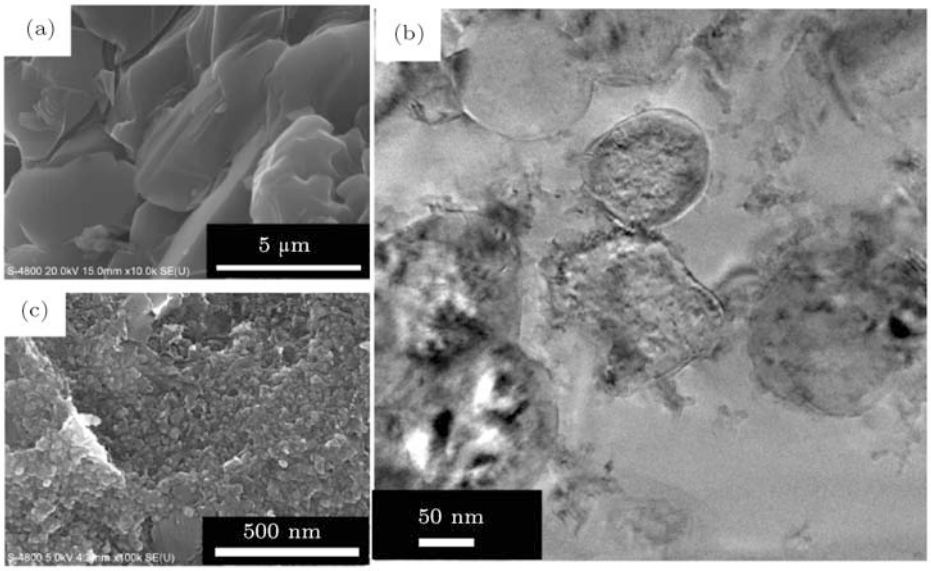


Fig. 3. FESEM and TEM of nanocomposites: (a) N0, (b) N50, and (c) N100.

3.2. Electrical transport properties

Table 1 shows the transport properties of the prepared nanocomposites at room temperature and a comparison is carried out with those cited from other reports. The value of $R_{\rm H}$ for the sample is negative, indicating that the conductivity is due mainly to electrons. The carrier concentration shows a small decrease according to the increase of nanopowder content, which can be attributed to the increased grain boundary scattering introduced by the higher amounts of nanopowder content. The carrier concentrations of our samples are much higher than that of Sb-doped Mg_2Si (10^{19} cm^{-3}) reported by Tani[1] and that of Bi-doped Mg_2Si (10^{20} cm^{-3}) reported by Akasaka.[23] This may indicate that the impurities in our samples are nearly fully ionized at room temperature and hence it shows little change in the measured temperature range. Figure 4 shows the temperature dependences of electrical conductivity of σ of Mg_2Si nanocomposites. The electrical conductivities of all samples increase with temperature increasing over the measured temperature range, which is in contrast to the trends given in other reports.[1,22] It is known that σ is defined by $\sigma = ne\mu$ (n is the carrier concentration and μ is the carrier mobility) and that the temperature dependence of mobility in $Mg_2Si_xGe_{1-x}$ compound[23,24] fulfills the relationship of $\mu \propto T^{-3/2}$, where acoustic lattice scattering is the predominant mechanism. Therefore, σ decreases with temperature increasing due to the decrease of mobility with temperature increasing. However,in the present work, the scattering mechanism may be dependent primarily on ionized impurity scattering and acoustic lattice scattering resulting from a relatively high number of carriers and more grain boundaries and, therefore, the mobility can be expressed as[25]

$$\mu = \frac{e}{m^*}\frac{1}{AT^{3/2} + \dfrac{BN_{\rm i}}{T^{3/2}}}, \tag{1}$$

where e is the electron charge, m^* is the electron effective mass, T is the absolute temperature, and $N_{\rm i}$ is the impurity concentration.

Table 1. Hall measurements of our nanocomposites at room temperature compared with those cited from other reports.

Sample	Conduction type	Carrier concentration /10^{19} cm^{-3}	Mobility /cm^2·V^{-1}·s^{-1}
N0	N	8.1	11.05
N20	N	6.5	9.01
N50	N	5.59	7.04
N80	N	4.64	4.60
N100	N	4.2	1.10
0.5at% Sb-doped Mg_2Si[1]	N	7.6	98.0
0.5at% Bi-doped Mg_2Si[23]	N	7.92	132.6

In lower temperature ranges, ionized impurity scattering plays a primary role, owing to a fairly high value of $N_{\rm i}$, and then the temperature dependence of mobility can be denoted by $\mu \propto T^{3/2}$ and n is nearly stable, consequently σ increases sharply with temperature increasing. However, in a higher temperature range, the slope of the increase of σ becomes slow, owing to $BN_{\rm i}/T^{3/2}$ decreasing with the increase of temperature.

From Fig. 4, it can be seen that the electrical conductivity σ of the nanocomposite decreases with the increase of amount of nanoscale powder content, and it can be attributed to higher density of grain boundaries induced by nanoscale powder in nanocomposites which enhance the scattering of carriers.

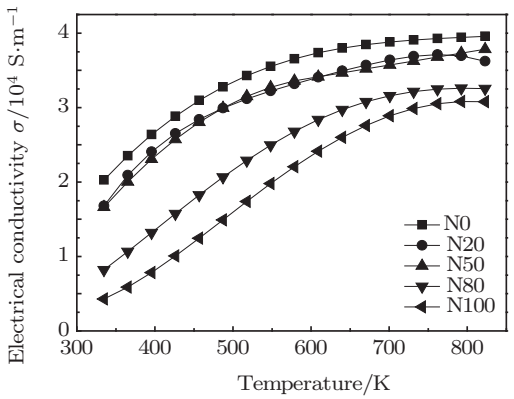


Fig. 4. Temperature dependences of electrical conductivity of the nanocomposites with different amounts of nanopowder content.

The Seebeck coefficient α that is plotted as a function of temperature from room temperature to about 823 K is shown in Fig. 5. All samples exhibit n-type conduction, which confirms the results of Hall measurement. The Seebeck coefficient of the nanocomposite basically increases with the increase of nanopowder inclusions. The results reported by Kishimoto and Koyanagi have demonstrated that the Seebeck coefficient increases with the decrease of grain size in PbTe compounds due to the potential barrier scattering of grain boundaries.[26,27] In the present case, we assume that the relaxation time approximation holds true and that the relaxation time τ of a carrier is given by $\tau = \tau_0 \varepsilon^r$, where ε is the carrier energy, τ_0 is the energy independent factor of the relaxation time and r is the scattering parameter. Then the Seebeck coefficient of a homogeneous material, which contains no grain boundaries, is given by[26]

$$S = \frac{\kappa}{e}\left[\frac{(r+5/2)F_{r+3/2}(\eta^*)}{(r+3/2)F_{r+1/2}(\eta^*)} - \eta^*\right], \qquad (2)$$

where κ is the Boltzmann's constant, η is the Fermi energy, $\eta^*(=\eta/\kappa T)$ is the reduced Fermi energy and F is the Fermi–Dirac integral. This equation indicates that the Seebeck coefficient is dependent basically on only two parameters: the Fermi energy and the scattering parameters.

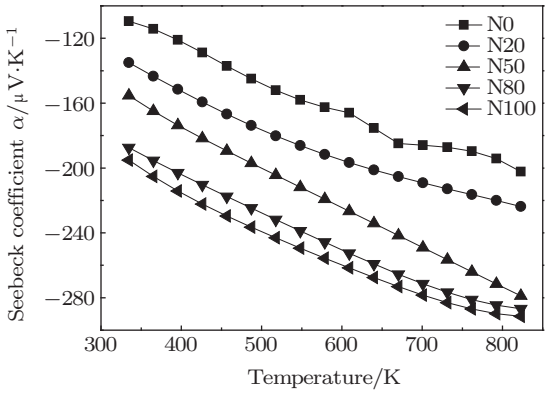


Fig. 5. Temperature dependences of the Seebeck coefficient of the nanocomposite with different amounts of nanopowder content.

First, we discuss the influence of the Fermi energy on the Seebeck coefficient. As seen in Table 1, the carrier concentration decreases with the increase of nanopowder content. This decrease in carrier concentration probably leads to a decrease in Fermi energy, which can increase the Seebeck coefficient. Figure 6 shows the relationship between Seebeck coefficient, carrier concentration and grain sizes of our nanocomposites at room temperature, and the values reported in Ref. [28] are presented too. It shows that the changes of Seebeck coefficient are not obvious for both samples containing large sized powder and nanopowder. It indicates that the decrease in carrier concentration makes little contribution to the increase of Seebeck coefficient.

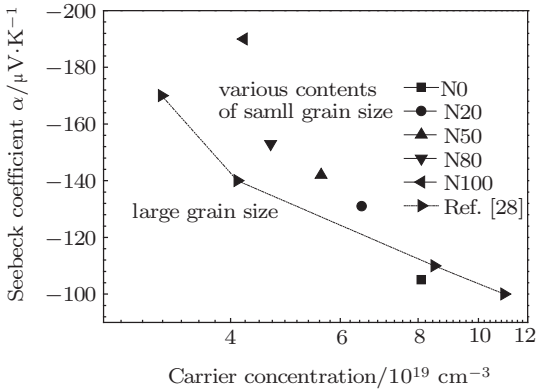


Fig. 6. Curves for the Seebeck coefficient of our nanocomposites as a function of carrier concentration at room temperature compared with that of the large grain-size samples reported in Ref. [28].

Second, we examine the influence of scattering parameters r on the Seebeck coefficient. For a degenerate material ($\eta^* \geq 1$), equation (2) becomes[29]

$$S = \frac{\pi^2}{3}\frac{\kappa}{e}\frac{(r+3/2)}{\eta^*}. \tag{3}$$

By using this equation, we calculate the Seebeck coefficient of Bi-doped Mg_2Si,[28] whose carrier concentration is similar to that of our sample, for several values of scattering parameter r. The results are plotted in Fig. 7, where the Seebeck coefficient of our nanocomposite is also plotted for comparison. This figure indicates that our sample N0, whose grain size is large, exhibits a Seebeck coefficient similar to that calculated for $r = -1/2$. This is consistent with the fact that the main scattering mechanism in Mg_2Si, which has a sufficiently large grain size or shows little effect from grain boundaries, is acoustic phonon scattering. The figure also indicates that a larger scattering parameter r, which is dependent on grain size, can cause the Seebeck coefficient to increase. However, ionized impurity scattering ($r = 3/2$) and optical phonon scattering ($r = 1/2$) cannot be such a scattering mechanism because these two scatterings occur regardless of grain size. Neutral impurity scattering ($r = 0$) may be intensified by a reduction of grain size because the reduction may induce a number of defects, which may cause this scattering into the grain and the grain boundary regions. However, from Fig. 7, it also shows that neutral impurity scattering ($r = 0$) cannot explain the increase in Seebeck coefficient. Thus, potential barrier scattering is the only likely cause of the increasing Seebeck coefficient with the increase nanopowder content.

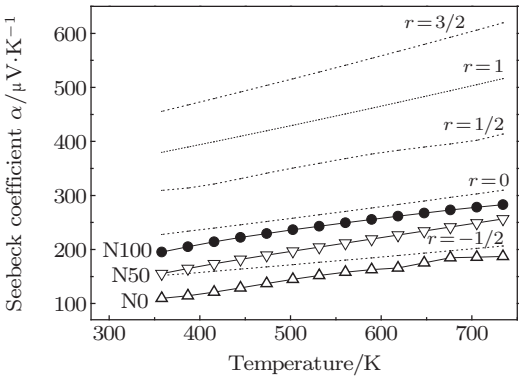


Fig. 7. Temperature dependences of the Seebeck coefficient of Bi-doped Mg_2Si material, calculated using Eq. (3) for various r values, where the carrier concentration is 4.1×10^{19} cm^{-3}, indicated by the broken lines. The point and solid lines indicate our samples.

3.3. Thermal transport properties

The most attractive aspect of nanocomposites are their low thermal conductivities. The values of thermal conductivity (κ) for all samples are shown in Fig. 8(a), each as a function of temperature. It shows that κ of a nanocomposite basically decreases with the increase of nanopowder content in the whole measured temperature range. The lower thermal conductivities of samples with more amounts of nanopowder content are due to the small grain size. The model usually proposed to understand the effect on thermal conductivity of grain size is the relaxation time approach to boundary scattering based on the Callaway theory.[30] Nan and Birringer[31] have adopted an approximation: the thermal conductivity κ is given by $1/\kappa = 1/\kappa_0 + 2R_k/D$, where κ_0 is the bulk thermal conductivity; R_k is the Kapitza resistance, which is almost independent of temperature and is 1.0×10^8 m^2·W/K for our samples based on the Kapitza resistance — EMA method;[31] D is the average grain size. One may anticipate that κ can further decrease if even smaller grain sizes are achieved.

Furthermore, thermal conductivities of all samples decrease with the increase of temperature in the measured temperature range. As is well known, κ is the sum of the contributions arising from the lattice ($\kappa_{\rm ph}$) and electronic ($\kappa_{\rm el}$) components,[32] and $\kappa_{\rm el}$ can be calculated using the Wiedemann–Franz law[33]

$$\kappa_{\rm el} = L\sigma T, \tag{4}$$

where L is the Lorentz number (here it is 2.45×10^{-8} V^2/K^2), σ is the electrical conductivity and T is the absolute temperature. The value of $\kappa_{\rm ph}$ is obtained by subtracting $\kappa_{\rm el}$ from κ. Figures 8(b) and 8(c) show the temperature dependences of $\kappa_{\rm el}$ and $\kappa_{\rm ph}$ of Mg_2Si nanocomposites, respectively. The value of $\kappa_{\rm el}$ increases with the increase of temperature, which results from the increase of electrical conductivity with temperature increasing. For N0 sample, the ratio of $\kappa_{\rm el}$-to-$\kappa_{\rm ph}$ is 1/50 at 300 K and about 1/4 at 823 K; for N50 sample, the ratio of $\kappa_{\rm el}$-to-$\kappa_{\rm ph}$ is 1/50 at 300 K and about 1/25 at 823 K. In most kinds of thermoelectric compounds, the relatively high thermal conductivity is mainly because of the high phonon contribution.[34] In the present study, it can also be seen that $\kappa_{\rm ph}$ makes the primary contribution to κ. The decrease in the total thermal conductivity of the nanocomposite is due mainly to the phonon part. This provides further evidence that nanostructuring will reduce the phonon thermal conductivity of the material

due to the enhanced scattering at grain boundaries.

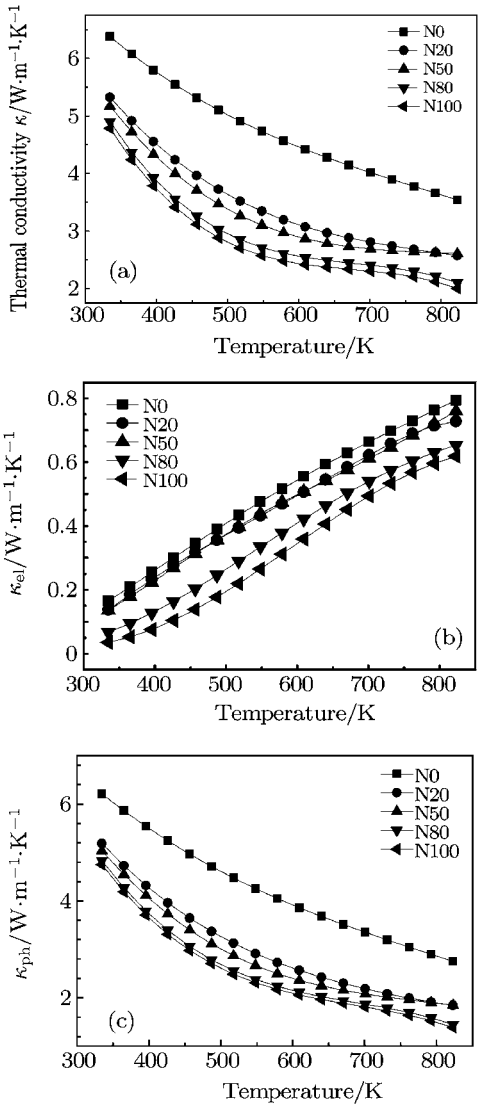


Fig. 8. Temperature dependences of thermal conductivity κ (a), $\kappa_{\rm el}$ (b), and $\kappa_{\rm ph}$ (c) of the nanocomposites with different amounts of nanopowder content.

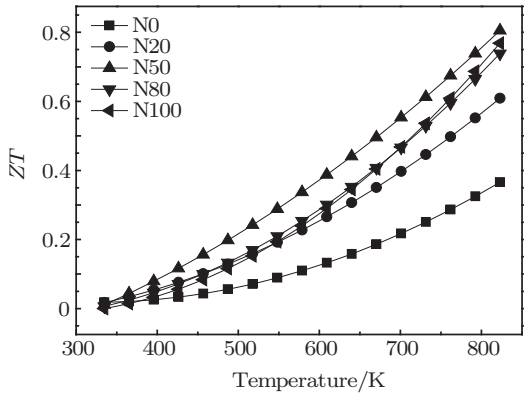


Fig. 9. Temperature dependences of ZT of the nanocomposties with different amounts of nanopowder content.

The dimensionless figure of merit ZT is calculated and discussed in Fig. 9. Taking the values of σ, α, and κ into consideration, a maximum ZT of 0.8 is obtained at 823 K for the sample of N50 with 50-wt% nanopowder, which is about 63% higher than that of Mg_2Si sample without nanopowder. The enhanced thermoelectric properties of the Mg_2Si nanocomposites confirm the effect of nanocomposite structure, which induces the larger reduction of κ and the enhancement of α.

4. Conclusion

N-type Mg_2Si nanocomposites are prepared by spark plasma sintering of a mixture of microsized and nanoscale Mg_2Si powders. The results show that the nanocomposite structures are effective to reduce the thermal conductivity and enhance the Seebeck coefficient, and hence the thermoelectric properties are improved. The maximum dimensionless figure of merit is enhanced to 0.8 at 823 K for Bi-doped Mg_2Si when nanopowders and micrometer-sized powders are mixed at the same ratio, which is about 63% higher than that of Mg_2Si without a nanocomposite structure.

References

[1] Junichi T and Hiroyasu K 2007 *Intermetallics* **15** 1202
[2] Rong R B, Aizawa T and Sun J Q 2007 *Mater. Sci. Eng.* B **136** 111
[3] Ratai E and Augustine M P 2003 *J. Phys. Chem.* B **107** 12573
[4] Morris R G, Redin D and Danielson G C 1958 *Phys. Rev.* **109** 1909
[5] Kajikawa T, N Kimura and Yokoyama T 2003 *Proceedings ICT*' 03 August 17–21 2003 Palais des Congrks La Grande Motte, France p. 305
[6] Aizawa T and Song R 2006 *Intermetallics* **14** 382
[7] Fedorov M I, Zaitsev V K and Vedernikov M V 2006 *Proceedings ICT*' 06 August 6–10 2006 Vienna, Austria p. 111
[8] Yu B L, Qi Q, Tang X F and Zhang Q J 2005 *Acta Phys. Sin.* **54** 5763 (in Chinese)
[9] Tang X F, Chen L D and Goto T 2000 *Acta Phys. Sin.* **49** 2437 (in Chinese)
[10] Hsu K F, Loo S, Guo F, Chen W, Dyck J S, Uher C, Hogan T, Polychroniadis E K and Kanatzidis M G 2004 *Science* **303** 818
[11] Zhao X B, Ji X H, Zhang Y H, Zhu T J, Tu J P and Zhang X B 2005 *Appl. Phys. Lett.* **86** 062111
[12] Martin J, Nolas G S, Zhang W and Chen L 2007 *Appl. Phys. Lett.* **90** 222112
[13] Yang R G and Chen G 2004 *Phys. Rev.* B **69** 195316
[14] Dresselhaus M S, Chen G, Tang M Y, Yang R, Lee H, Wang D, Ren Z, Fleurial J and Gogna P 2007 *Adv. Mater.* (Weinheim, Ger.) **19** 1043
[15] Wang L and Qin X Y 2003 *Scripta Materialia* **49** 243
[16] Riffel M and Schilz J 1995 *Scripta Metallurgica et Materialia* **32** 1951

[17] Wang L and Qin X Y 2007 *Mater. Sci. Eng.* A **459** 216
[18] Lee C H, Lee S H, Chun S Y and Lee S J 2006 *J. Nanosci. Nanotechnol.* **6** 3429
[19] Szczech J R and Jin S 2008 *J. Solid State Chem.* **181** 1565
[20] Zhang Q, He J, Zhu T J, Zhang S N, Zhao X B and Tritt T M 2008 *Appl. Phys. Lett.* **93** 102109
[21] Huang J W 2006 *MDI Jade Users Handbook* (Changsha: Central South University Press) p. 33 (in Chinese)
[22] Akasaka M, Iida T, Matssumoto A and Yamanaka K 2008 *J. Appl. Phys.* **104** 013703
[23] LaBotz R J, Mason D R and O'Kane D F 1963 *J. Electrochem. Soc.* **110** 127
[24] Noda Y, Kon H, Furukawa Y and Otsuka N 1992 *Mater. Trans. JIM* **33** 851
[25] Liu E K, Zhu B S and Luo J S 1989 *Semiconducting Materials* (Beijing: National Defence Industry Press) p. 497 (in Chinese)
[26] Kishimoto K and Koyanagi T 2002 *J. Appl. Phys.* **92** 2544
[27] Moizhes B Ya and Nemchinsky V 1992 *Proceedings ICT*' 92 October 7–9 1992 Arlington, Texas, USA p. 232
[28] Tani J and Kido H 2005 *Physica* B **364** 220
[29] Goldsmid H J 1998 *Electronic Refrigeration* (Lodon: Pion) Vol. 2 p. 36
[30] Callaway 1959 *J. Phys. Rev.* **57** 1046
[31] Nan C W and Birringer R 1998 *Phys. Rev.* B **57** 8264
[32] Bhandari C M 1995 *CRC Handbook of Thermoelectric* ed. Rowe D M (New York: CRC Press) p. 57
[33] Deng S K, Tang X F and Zhang Q J 2007 *Acta Phys. Sin.* **56** 4986 (in Chinese)
[34] Morelli D T and Caillat T 1995 *Phys. Rev.* B **51** 9622